Cell Reports
Physical Science

CellPress
OPEN ACCESS

Article

Ferromagnetic supramolecular metal-organic frameworks for active capture and magnetic sensing of emerging drug pollutants

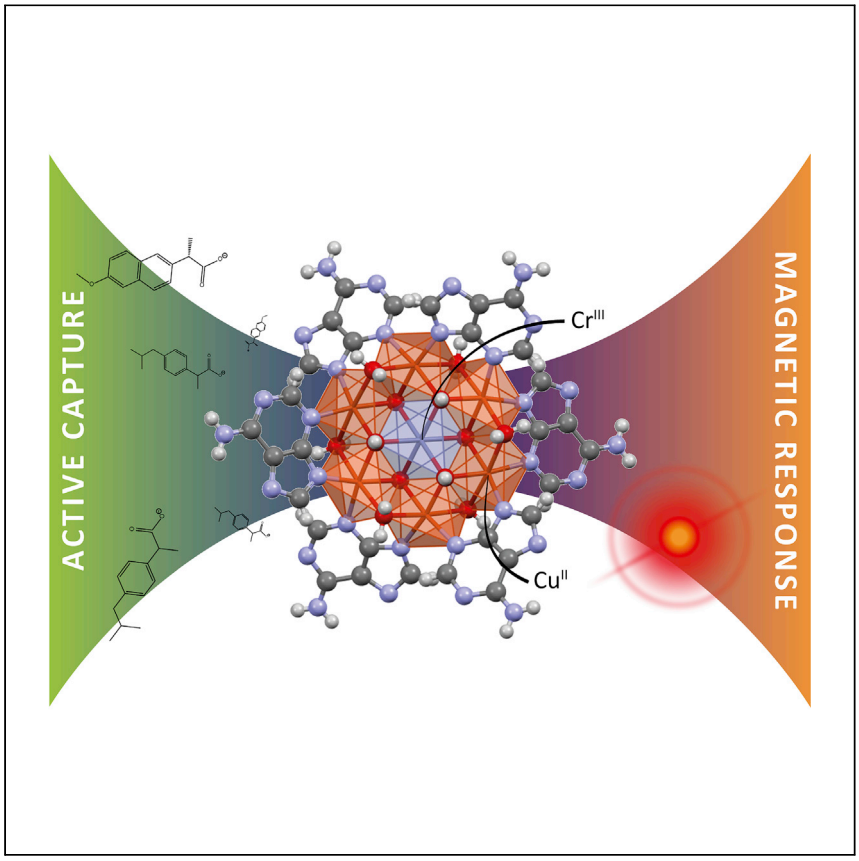

Ferromagnetic supramolecular metal-organic frameworks are capable of capturing anionic drugs from very dilute solutions and provide a magnetic response that can be used to quantify the captured amount. Pérez-Aguirre et al. report the use of a $CrCu_6$ SMOF to quantifiably detect anionic drugs using its room temperature paramagnetic properties.

Rubén Pérez-Aguirre, Beñat Artetxe, Garikoitz Beobide, ..., Antonio Luque, Sonia Pérez-Yáñez, Stefan Wuttke

oscar.castillo@ehu.eus (O.C.)
stefan.wuttke@bcmaterials.net (S.W.)

Highlights

SMOF reversible room temperature assembly/disassembly allows active drug capture

Inert Cr(III) ions forming $CrCu_6$ species lead to enhanced magnetic response

Room temperature paramagnetic properties of SMOF allow facile magnetic sensing

Potential application for environmental remediation and emerging pollutants monitoring

Pérez-Aguirre et al., Cell Reports Physical Science *2*, 100421
May 19, 2021
https://doi.org/10.1016/j.xcrp.2021.100421

Cell Reports
Physical Science

CellPress
OPEN ACCESS

Article

Ferromagnetic supramolecular metal-organic frameworks for active capture and magnetic sensing of emerging drug pollutants

Rubén Pérez-Aguirre,[1] Beñat Artetxe,[1] Garikoitz Beobide,[1,2] Oscar Castillo,[1,2,6,7,*] Imanol de Pedro,[3] Antonio Luque,[1,2] Sonia Pérez-Yáñez,[1,2] and Stefan Wuttke[2,4,5,*]

SUMMARY

Capture and sensing of emerging pollutants is one of the increasing environmental concerns due to the adverse ecological and human health effects. Here, we report the synthesis of a supramolecular metal-organic framework (SMOF) $[CrCu_6(\mu\text{-}H_2O)_6(\mu_3\text{-}OH)_6(\mu\text{-adeninato-}\kappa N3_3{:}\kappa N9)_6](SO_4)_{1.5}$ which is able to capture anionic drugs and exhibits magnetic properties useful for sensing purposes. The features of the nucleobase decorated $CrCu_6$ building block allow the incorporation of up to 9 drug molecules (i.e., ibuprofen and naproxen in this work) per heptameric entity. In addition, we provide a simple way to quantify the incorporated number of drug molecules through a magnetic sustentation experiment in which the field required to keep the particles attached to the electromagnet pole is linearly related to the total mass of the anionic counterion. In this way, it also provides an easy way to determine the amount of entrapped drug molecules, making this SMOF a promising candidate for environmental remediation technologies.

INTRODUCTION

Emerging pollutants (pharmaceutical, agricultural, and industrial) detected in many aquatic matrices (groundwater, wastewater, and drinking water) are one of the increasing environmental concerns due to the adverse ecological and human health effects.[1] Among them, pharmaceutical pollutants such as drugs are released into the environments by domestic wastewaters and pharmaceutical sewage without any regulation, leading to the increased level of pollution that may affect living organisms.[2] Therefore, developing facile methods to eliminate drugs from water media and effective methodologies to analyze their quantities is a crucial issue.

In this work, we focus on the development of a methodology to efficiently capture anionic drugs, in particular the widely prescribed anti-inflammatory medicines ibuprofen and naproxen, and quantitatively analyze their number. Among all of the techniques explored so far, the one based on adsorbents is considered one of the most appropriate options, given that it shows an excellent removal capacity.[3] More specifically, up to now, the most commonly used adsorbents have been activated carbon, zeolites, mesoporous silica, cyclodextrins, and chitosan beads.[4] In this challenging quest for the ideal adsorbent, metal-organic frameworks (MOFs) have emerged as a suitable platform.[5] These ordered crystalline porous materials are renowned due to their high surface areas, tunable pores, well-defined channels, facile loading, and intriguing functionalities, which allow them to fulfill several applications.[6–10]

[1]Departamento de Química Inorgánica, Universidad del País Vasco, UPV/EHU, Leioa, Biscay, Spain

[2]Basque Center on Materials, Applications and Nanostructures, BCMat, UPV/EHU Parque de Científico, 48940 Leioa, Spain

[3]Universidad de Cantabria, CITIMAC, Facultad de Ciencias, Avenida de los Castros s/n, 39005 Santander, Spain

[4]IKERBASQUE, Basque Foundation for Science, 48009 Bilbao, Spain

[5]Twitter: @wuttkescience

[6]Twitter: @OscarCa38710720

[7]Lead contact

*Correspondence: oscar.castillo@ehu.eus (O.C.), stefan.wuttke@bcmaterials.net (S.W.)

https://doi.org/10.1016/j.xcrp.2021.100421

A related burgeoning field is that of supramolecular metal-organic frameworks (SMOFs), in which the coordination bonds are released from guiding the crystal structure, and supramolecular interactions (π-π stacking interactions and/or hydrogen bonds) play this role instead.[11] The hallmark feature of SMOFs in comparison with MOFs is their facile assembling/disassembling reversibility at room temperature due to the protonation/deprotonation of ligands, which may be used for the incorporation of various species. Meanwhile, SMOFs exhibiting magnetic properties are highly promising, not only for molecule capture but also for their facile sensing.

As previously mentioned, monitoring drug molecules is important for the quantitative evaluation of the pollution level. Conventional analytical methods to quantify adsorbed molecules mainly include solid-phase extraction (SPE) or liquid-liquid extraction (LLE) coupled with chromatographic or chromatographic-mass spectrometry techniques. However, the selectivity and sensitivity of these methods are often not sufficient for the direct determination of pollutants at very low concentrations.[12] Therefore, alternative analysis methods are in high demand.[13]

Magnetic solid-phase extraction (MSPE) is an emerging type of SPE based on the dispersing of magnetic adsorbents in the solution of targeted compounds.[14–16] This technique uses an external magnetic field to isolate adsorbents with targeted compounds. Eventually, analytes can be eluted from the adsorbent surface with various solvents for the consequent analysis. In contrast to the conventional SPE techniques, MSPE does not require time-consuming processes such as column passing, filtration, or centrifugation. It is also advantageous due to its simplicity, low cost, higher efficiency, selectivity, sensitivity, and recyclability of most adsorbents. Therefore, synthesizing magnetic adsorbents and using the MSPE method to evaluate the concentration of the adsorbed species is of high interest.

Recently, we reported the synthesis of bioinspired SMOF $[Cu_7(\mu\text{-}H_2O)_6(\mu_3\text{-}OH)_6(\mu\text{-adeninato-}\kappa N3{:}\kappa N9)_6](NHEt_3)_2(SO_4)_2$, which combines intrinsic porosity with interesting magnetic features.[17] In this compound, the heptanuclear $Cu_7(\mu\text{-}H_2O)_6(\mu_3\text{-}OH)_6(\mu\text{-adeninato-}\kappa N3{:}\kappa N9)_6]^{2+}$ wheels are joined together by means of π-π stacking interactions, and the central $[Cu(OH)_6]^{4-}$ core is antiferromagnetically coupled to the external ferromagnetic Cu_6 ring, leading to a S = 5/2 ground state. The above-mentioned heptanuclear entity has been recurrently described in some other SMOFs,[18,19] and it has been recently reported as a building unit of a MOF.[20] Worthy of mention is the case of SMOFs that can accommodate different types of anionic species due to the nature and size of their voids. The molecular recognition capacity provided by the adeninato ligands decorating the outer surface of the wheel-shaped heptamer allows the incorporation of both organic and inorganic guests.[17–19]

In this study, we propose a facile synthesis of SMOF $[CrCu_6(\mu\text{-}H_2O)_6(\mu_3\text{-}OH)_6(\mu\text{-adeninato-}\kappa N3{:}\kappa N9)_6](SO_4)_{1.5}$ with maximized magnetic properties in comparison with the previously reported SMOF with heptameric Cu_7 species. The enhanced magnetic interaction is achieved by introducing kinetically inert Cr(III) ions, forming $CrCu_6$ species. Meanwhile, the protonation/deprotonation of adenine nucleobases leads to room temperature (RT) reversible assembly/disassembly, enabling efficient drug capture during SMOFs reassembly. Moreover, the synthesized compound exhibits paramagnetic properties at RT, which are used to develop a novel type of MSPE for the adsorbed molecule quantification. To be more specific, SMOFs with adsorbed ibuprofen and naproxen molecules in liquid media are exposed to the

variable magnetic field, and the number of adsorbed molecules is determined by the strength of the applied magnetic field required to attract the particles suspended in a liquid.

RESULTS AND DISCUSSION

Design and synthesis of SMOF

Encouraged by the appealing molecular and magnetic properties displayed by $[Cu_7(\mu\text{-}H_2O)_6(\mu_3\text{-}OH)_6(\mu\text{-adeninato-}\kappa N3{:}\kappa N9)_6](NHEt_3)_2(SO_4)_2$, a new heterometallic SMOF of formula $[CrCu_6(\mu\text{-}H_2O)_6(\mu_3\text{-}OH)_6(\mu\text{-adeninato-}\kappa N3{:}\kappa N9)_6](SO_4)_{1.5}$, has been designed and synthesized to maximize the magnetic response and simultaneously increase its chemical stability due to the well-known inertness of the Cr(III) octahedral complexes. The synthesis required a fine-tune between the pH value of the reaction media and the proportions of the reagents (see Experimental procedures for more details). According to our expectations, we achieved the above-mentioned $CrCu_6$ heptanuclear unit, in which the central position is now occupied by Cr(III). Note that despite Cu(II) metal atoms in the pristine material presenting an octahedral geometry with the usual Jahn-Teller tetragonal elongation, the rigidity of the wheel-shaped heptanuclear entity provokes a less pronounced Jahn-Teller effect for the central atom. This, in turn, favors the replacement of the central position by Cr(III) and promotes the formation of the heterometallic $[CrCu_6(\mu\text{-}H_2O)_6(\mu_3\text{-}OH)_6(\mu\text{-adeninato-}\kappa N3{:}\kappa N9)_6]^{3+}$ ($CrCu_6$) species (Figure 1). Each heptanuclear entity acts as a 4-connected node, in which the π-π stacking interactions between adeninato ligands provide a supramolecular porous architecture (44.3% of unit cell volume) with cds ($CdSO_4$-like) topology and ($6^5.8$) point symbol.[21] Full characterization and detailed structural description are given in the Supplemental information (Figures S2–S4; Table S3).

Magnetic properties clearly differ with respect to the homometallic Cu_7 analogs as the orthogonality between the Cr(III) t_{2g} and Cu(II) e_g magnetic orbitals leads to the ferromagnetic S = 9/2 ground state instead of the ferrimagnetic S = 5/2 ground state of the Cu_7 analogs. The molar magnetic susceptibility (χ_M) and the $\chi_M T$ product for $CrCu_6$, measured at 1 kOe after cooling without an applied magnetic field (zero field cooled [ZFC]) together with the magnetization curve at 2 K are gathered in the Supplemental information. The $\chi_M T$ value increases as temperature decreases from RT, which is associated with intramolecular ferromagnetic interactions. A plateau is achieved between 7 and 40 K with the $\chi_M T$ value ~12.72 emu K/mol Oe (close to the theoretical 12.375 emu K/mol Oe value for a S_T = 9/2 and g = 2.0). Below 7 K, the $\chi_M T$ value decreases sharply, probably due to intermolecular antiferromagnetic interactions, similar to those observed in the homometallic Cu heptamers.[17]

The fitting of the $\chi_M T$ data (Figures S5 and S7) was performed using the MagProp software tool distributed with DAVE.[22] The resulting magnetic coupling constants (J_1 = +80 and J_2 = +51 cm^{-1}; g = 2.04; zJ' = −0.024 cm^{-1}) are in concordance with the magnetic topology inferred from the saturation magnetization of $CrCu_6$ clusters. In general terms, peripheral Cu(II) atoms are ferromagnetically coupled ($J_1 > 0$) due to the countercomplementarity between the magnetic orbitals induced by the double bridge adenine/hydroxide.[22] The obtained magnetic coupling values for both magnetic pathways lie within the range described in the references.[17–19,23–25]

Although this compound establishes complex magnetic interactions at low temperatures, at RT, it is well placed in the paramagnetic regime. Therefore, the attraction force exerted by a relatively strong external magnetic field (i.e., that of magnets or

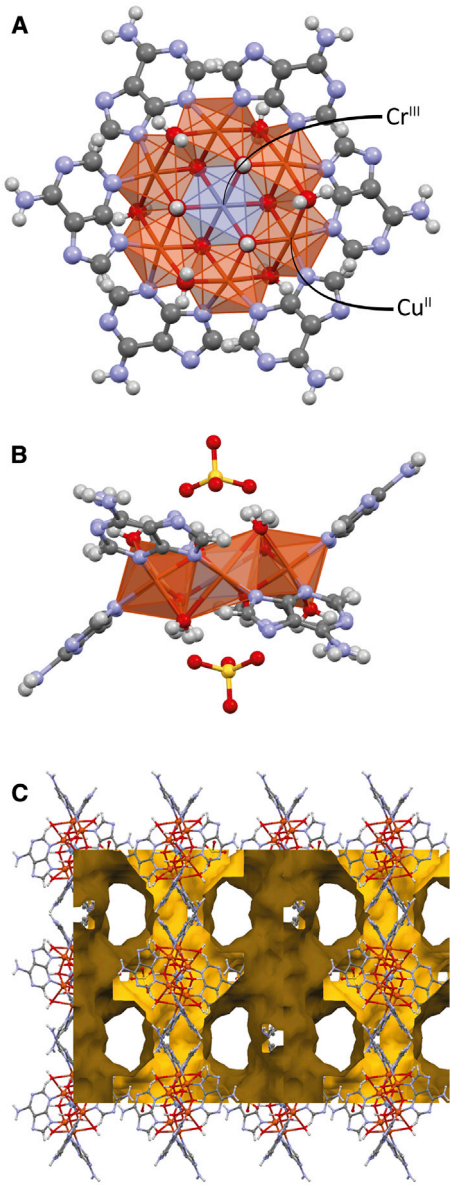

Figure 1. Structure of SMOF $[CrCu_6(\mu\text{-}H_2O)_6(\mu_3\text{-}OH)_6(\mu\text{-adeninato-}\kappa N3{:}\kappa N9)_6]^{3+}$
(A) $[CrCu_6(\mu\text{-}H_2O)_6(\mu_3\text{-}OH)_6(\mu\text{-adeninato-}\kappa N_3{:}\kappa N_9)_6]^{3+}$ heptameric discrete entity.
(B) Lateral view of the heptameric entity showing the interacting SO_4^{2-} counterions.
(C) Porous supramolecular architecture showing the voids within the crystal structure.

electromagnets) on the particle of the samples is too weak to overcome the earth gravity attraction under normal conditions, and as a consequence, no displacement takes place on these particles.

However, under reduced gravity conditions, such as when the particles are immersed in a liquid, the magnetic field attraction can be strong enough to avoid them from depositing at the bottom and even to promote their motion (Figure 2). The equation mediating the attraction force between the paramagnetic particles and the magnetic field implies $F = \nabla (m \cdot H)$, where the gradient ∇ is the change of the $m \cdot H$ product per unit of length m: magnetic dipole of the particle and

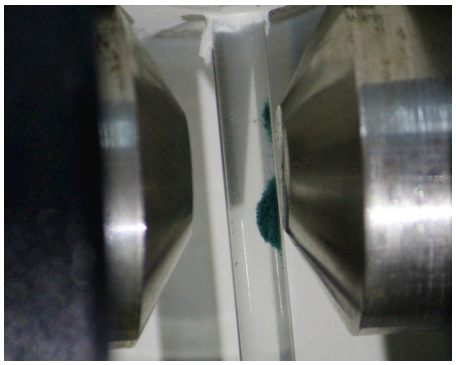

Figure 2. Magnetic field attraction at room temperature
Particles immersed in methanol attached to the poles of an electromagnet.

H: external magnetic field, and the direction is that of the maximum increase of $m \cdot H$. If *m* is in the same direction as *H*, as it happens for paramagnetic particles, then the gradient pulls the particles into regions of maximum *H* field.[26] This equation is strictly only valid for zero-size magnets, but it is often a good approximation for tiny particles, as in this case. Taking into account the paramagnetic nature of the particles, their magnetic dipole can be expressed based on the external magnetic field and taken away from the gradient as the particles are so small that the magnetic dipole moment can be considered constant all along the particle (Equation 1):

$$F_P = \mu_0 \frac{\chi_M}{MW} \cdot \rho_P \cdot V_P \cdot H \cdot \nabla(H) \qquad \text{(Equation 1)}$$

where F_P is the magnetic attraction force on the particle, μ_0 is the permeability of the vacuum, χ_M is the molar susceptibility, *MW* is the molecular weight of the compound (excluding the solvent molecules located in the pores as they freely exchange with the media), ρ_P is the density of the compound, V_P is the particle volume, and *H* and ∇ (*H*) are the magnetic field and field gradient in the center of the particle, respectively. This implies that the magnetic force on the particles is not going to be uniform on the whole surface of the pole but that it achieves a maximum value on its edge pointing toward the central axis of the pole. It means that at the bottom of the pole perimeter, where the magnetic attraction force is opposite to the gravitation force, the particles of these compounds can accumulate, as can be observed in Figure 2. This phenomenon was corroborated using 3 different solvents: CCl_4, H_2O, and MeOH. The denser the solvent, the lower the magnetic field required to maintain the particles attached to the pole of the electromagnet.

All of the above-described features make this compound an appealing material, since it combines meaningful magnetic response even in the paramagnetic regime, a porous nature, and enhanced chemical stability. As a result, the molecules trapped within the voids will modify the material density, thereby altering the value at which the magnetic field is no longer able to sustain the particles of this compound. In addition to that, the rich acid-base chemistry of the adenine nucleobase allows us to dissolve the SMOF in acid aqueous solutions while retaining the molecular structure of the heptameric entities. Note that the bridging μ-κ*N3*:κ*N9* coordination mode leaves the pyrimidine N_1 and the imidazole N_7 positions of adeninato ligands as suitable acceptor positions for protonation without altering the key features of the wheel-shaped heptamer. This process was previously attempted with the homometallic Cu_7 analog, but its lability makes the acid media attack not only the base positions in the adeninato ligand but also the hydroxide anions that bridge the central metal atom to the peripheral ones, leading to its decomposition as clearly deduced from the adeninium sulfate precipitation. However, the presence of the inert Cr(III)

atom at the central position plays a crucial role as it provides kinetic inertness toward the protonation of the hydroxides, being the protonation taking place only at the nucleobases that are able to deal with it without collapsing the molecular structure of the heptameric entities. This feature allows its complete dissolution, which requires a pH close to 1.8. The obtained solution is stable for a few hours before the thermodynamically favored breakdown of the heptameric unit starts with the appearance of the previously mentioned adeninium sulfate precipitate. This fact confirms the kinetical stability of the CrCu6 entity in an acidic media. However, if the solution is not allowed to stand for such a long time at these very acidic pH values, for example by basifying with NaOH up to pH 6.5, then it again provides the starting compound with the same peculiar magnetic features provided by the presence of the $CrCu_6$ entity (Figures S10–S13; Table S4). More concisely, it can be stated that the heptanuclear entity is retained since the magnetization value of the recycled $CrCu_6$ compound remains at the expected values (M_s = 9.21) described for the pristine material. Moreover, the comparison between the thermogravimetric measurements of both $CrCu_6$ heptanuclear entities shows only a significant distinction on the amount of solvent present in each compound. All of the features corresponding to the heterometallic heptanuclear entity are also ensured by the similarity of the infrared (IR) spectra and by XPS (X-ray photoelectron spectroscopy) measurements. It should be noted here that the crystal structure of the reconstituted compound seems to be altered as deduced from its powder X-ray diffraction (PXRD) (Figure S14), but this polymorphism has been also reported for the homometallic Cu_7 analogs.[17–19]

Ibuprofen and naproxen drug molecule incorporation into SMOF

At this point, we decided to combine all of these features to provide a material that is able to actively entrap drugs of extensive use such as the anionic anti-inflammatory naproxen and ibuprofen molecules, which are a source of concern regarding water contamination.[27–31] These drugs have been selected because of their capability to form supramolecular interactions with the heptameric entity, either hydrogen bonding or π-π stacking interactions, but also because their anionic nature (pK_a = 4.2 and 5.3, respectively) allows the replacement of the SO_4^{2-} anions to balance the positive charge of the heptameric cluster. For this purpose, an acidic solution of the $CrCu_6$ heptamer is dropped into a solution containing these anionic drugs at concentrations of 248, 413, and 826 μM (corresponding to 51, 85, and 170 mg/L for ibuprofen and 57, 95, and 190 mg/L for naproxen; see the Supplemental information). The mixture of the $CrCu_6$ heptamer solution and the one containing the corresponding anionic drug leads to $CrCu_6$ heptamer:drug ratios of 1:6, 1:10, and 1:20. During the addition of the highly acidic solution of the heptamer, the pH of the solution was kept between pH 7 and 8 by the simultaneous addition of 1 M NaOH to prevent the precipitation of the highly insoluble neutral forms of the drugs. As the heptamer was added to the drug, a green suspension appeared but interestingly, the amount of precipitate clearly increased as the concentration of the drug solution increased. The integrity of the heptameric discrete units has been checked by XPS measurements (Figure S18). The bond energies of both the external ring Cu(II) and the central Cr(III) metal centers do not change, indicating that their immediate chemical environment remained unaltered. Additional characterization of the resulting precipitates (see the Supplemental information) indicated that the amount of the anionic form of the drug captured by the heptameric entities differs from 1:3 (for naproxen), 1:6 (for ibuprofen and naproxen), and 1:9 (for ibuprofen and naproxen).

The incorporation of a maximum of 9 monoanionic drug molecules per heptameric entity enables us to assume that in the acidic solution of $CrCu_6$, the heptameric entities have been able to incorporate 6 H^+, probably located on the non-coordinated

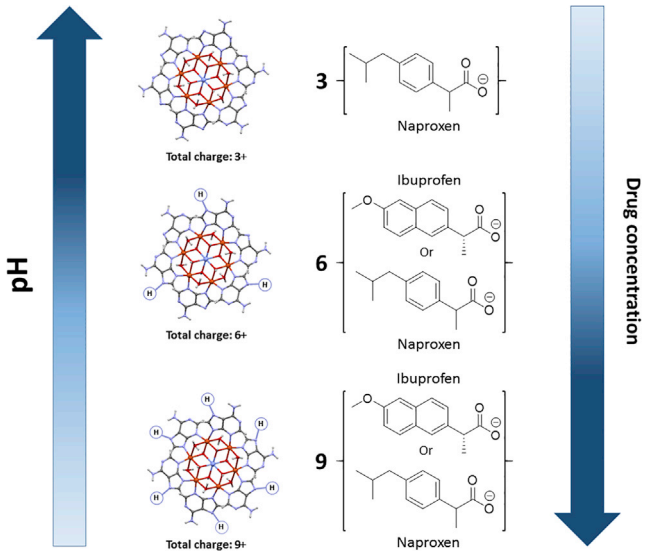

Figure 3. Drug active capture dependence toward pH and concentration
Relationship between the protonation of the adeninato ligand, the captured drug ratio per heptamer, and drug concentration in the batch.

endocyclic N_2 atoms of the adenines in such a way that the discrete entities acquire a 9+ charge, allowing us in turn to capture up to 9 anions of these drugs per formula. Apparently, depending on the concentration/ratio of the drug solution, the addition of these highly protonated 9+ entities into a nearly neutral solution leads to 2 competing processes: (1) the neutralization of these acidic entities and (2) their precipitation in the form of a cationic heptamer-anionic drug insoluble compound (Figure 3). At high drug concentrations, the second process takes place before any neutralization process, and it results in the isolation of H_6CrCu_6/ibuprofen 1:9 and H_6CrCu_6/naproxen 1:9 compounds. At intermediate concentrations, partial neutralization takes place before the anionic drug is able to precipitate it, giving rise to samples of H_3CrCu_6/ibuprofen 1:6 and H_3CrCu_6/naproxen 1:6 compounds. At the lower end of the concentrations, the neutralization can be completed for $CrCu_6$/naproxen 1:3, but for the ibuprofen analog, a mixture of the apparently 1:3 and 1:6 compounds is achieved. The incorporation of the drugs and the stoichiometry of the resulting products have been corroborated by means of Fourier transform IR (FTIR) spectroscopy, elemental analysis, and thermogravimetric analysis (TGA) measurements, as indicated in the Supplemental information. The capture efficiency decreases upon lowering the concentration and the $CrCu_6$:drug ratio, probably because the sulfate anion also provides an insoluble $CrCu_6$ species and competes with these anionic drugs (see Supplemental information for more details).

Magnetic sustentation experiments to sense the number of incorporated drug molecules

As previously stated, under the strong magnetic field generated by an electromagnet, the paramagnetic response of these compounds is enough to provide mobility to the particles immersed in a solvent and to attach them to the lower end of the magnetic pole. In this case, all of the samples contain the same paramagnetic heptameric $CrCu_6$ entity, but they differ on the nature and amount of the counterions. Thus, the variation of the magnetic field at which the sustentation of the particles ends will depend on the counterion total mass that makes the gravitation

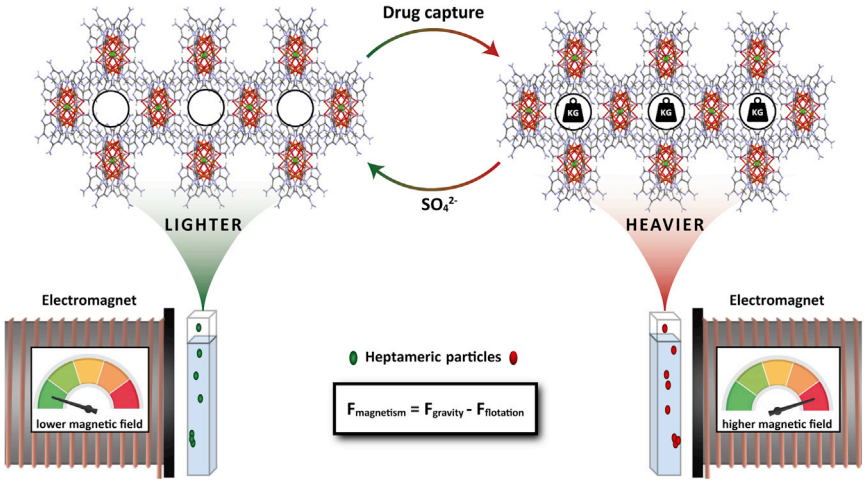

Figure 4. Schematic illustration of the magnetic sensing fundamentals

Influence of the replacement of the anionic part in the minimum magnetic force required to detach the particles from the magnetic pole during the magnetic sustentation experiments.

attraction increase and necessarily displaces the critical magnetic field toward higher values (Figure 4).

The use of an electromagnet provides a unique opportunity to exactly determine the minimum magnetic field required by each compound for their particles to fall from the pole bottom edge. According to Equation 1, it depends on the molecular susceptibility, which, in the paramagnetic regime, can be estimated using the spin-only expression depicted by Equation 2:

$$\chi_M = \frac{[4S_{Cr}(S_{Cr}+1)]+6\cdot[4S_{Cu}(S_{Cu}+1)]}{8T} \quad \text{(Equation 2)}$$

Furthermore, matching the magnetic and gravitation attraction forces, the exact magnetic field value at which the particles will fall from the pole can be calculated. However, one must bear in mind the flotation force exerted by the solvent on the particles, which only applies to the compound framework and not to the volume occupied by the pores of the material, as the molecules placed there freely exchange with the solvent. This leads to Equation 3:

$$\mu_0\frac{[4S_M(S_M+1)]+6\cdot[4S_{Cu}(S_{Cu}+1)]}{8T\cdot MW_F}\cdot\rho_F\cdot V_F\cdot H\cdot\nabla(H) = (\rho_F-\rho_S)\cdot V_F\cdot g \quad \text{(Equation 3)}$$

To find the dependence between the counterion total mass and the magnetic field required to keep the particles attached to the electromagnet pole, the volume occupied by the framework (V_F) in the particle must be divided into the volumes occupied by the heptameric entity (V_H) and by the counterions (V_C): $V_F = V_H + V_C$. The attraction of the magnetic field can be expressed only on V_H as it is the only source of the paramagnetism responsible for this attraction, but the gravitation-flotation part requires both terms V_H and V_C. Relating V_H and V_C, through the molecular density ρ_H and ρ_C and molecular weights ($MW_F = MW_H + MW_C$) of both components (Equation 4), Equation 5 is derived:

$$V_C = \frac{nMW_C\cdot\rho_H}{\rho_C\cdot MW_H}\cdot V_H \quad \text{(Equation 4)}$$

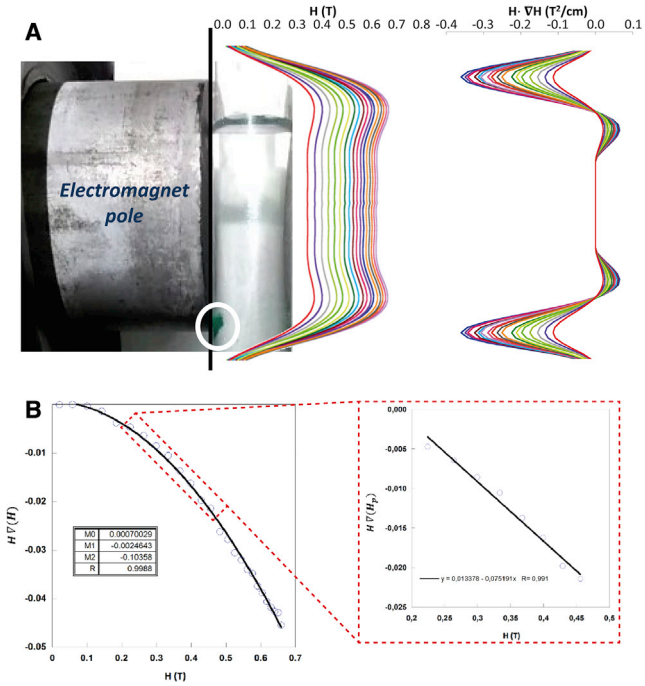

Figure 5. Magnetic field profile

(A) Magnetic field profile (H and $H \cdot \nabla(H)$) on the electromagnet pole along the dashed line. The different colors refer to the applied intensity current: increasing from 0.0 to 2.5 A (step: 0.1 A).
(B) $H \cdot \nabla(H)$ dependence on the magnetic field at the center of the pole. Left: second-order polynomial fitting of the entire magnetic field range; right: linear fit within the range at which the experimental data appear for these compounds.

$$\mu_0 \frac{[4S_{Cr}(S_{Cr}+1)]+6\cdot[4S_{Cu}(S_{Cu}+1)]}{8T\cdot MW_H}\rho_H \cdot V_H \cdot H\cdot\nabla(H) = \quad \text{(Equation 5)}$$

$$(\rho_H-\rho_S)V_H\cdot g + (\rho_C-\rho_S)\frac{nMW_C\cdot\rho_H}{\rho_C\cdot MW_H}\cdot V_H\cdot g$$

Isolating the total counterion mass (nMW_C)leads to Equation 6:

$$nMW_C = \mu_0 \cdot \rho_C \frac{[4S_{Cr}(S_{Cr}+1)]+6\cdot[4S_{Cu}(S_{Cu}+1)]}{8T\cdot(\rho_C-\rho_S)} H\cdot\nabla(H) - \frac{(\rho_H-\rho_S)g\cdot\rho_C\cdot MW_H}{(\rho_C-\rho_S)\rho_H} \quad \text{(Equation 6)}$$

Assuming that the counterions molecular density will not differ significantly and that the remaining parameters apart from nMW_C and $H \cdot \nabla(H_P)$ are constant, Equation 6 can be simplified into a linear equation with 2 constant terms (A and B) (Equation 7):

$$nMW_C = A\cdot H\cdot\nabla(H) + B \quad \text{(Equation 7)}$$

As can be deduced from Equation 7, to obtain information on the number of drug molecules captured by the heptameric units, it is necessary to know the magnetic field profile along the electromagnet pole and its variation when modifying the applied current (Figure 5).

According to Equation 7, the experimental data depicted on a nMW_C versus $H \cdot \nabla(H)$ graph fits satisfactorily to a straight line (Figure 6). The same can be observed if the experimental data are plotted on a nMW_C versus H graph due to the linear relationship between $H \cdot \nabla(H)$ and H for magnetic fields reported in the experiment (Figure 5B).

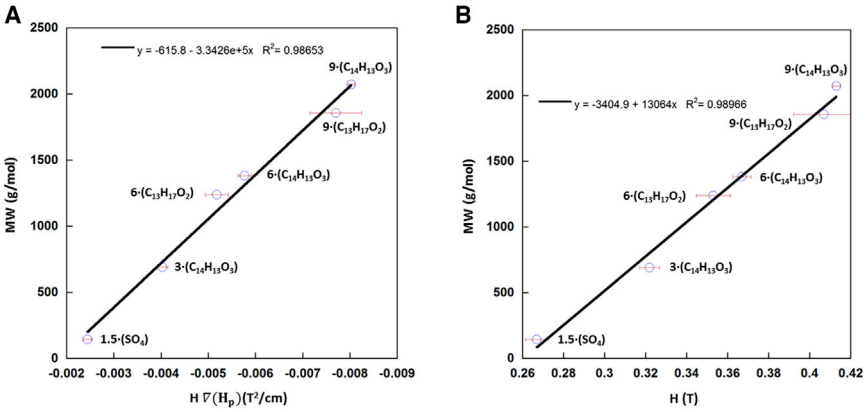

Figure 6. Linear dependencies of the magnetic field strength on molecular weight of the captured drug molecules

(A) Dependence of the molecular weight of the captured drug with respect to $H \cdot \nabla(H)$.

(B) Dependence of the molecular weight of the captured drug with respect to H.

In summary, the facile reversible assembling/disassembling capacity and the magnetic response of the herein reported ferromagnetic SMOF has allowed some unprecedented capabilities for this type of material. Making use of the features of the $CrCu_6$ building block, we have captured ibuprofen and naproxen with different stoichiometries: 1:3, 1:6, and 1:9, depending on the drug concentration. This fact is possible due to the different protonation states that the $CrCu_6$ building block can display without altering its molecular structure, which is directly related to the presence of multiple donor sites in the adenine nucleobase. Furthermore, focusing on the paramagnetic response at RT of the $CrCu_6$ entity, we have provided a simple way to quantify the incorporated number of drug molecules. In a magnetic sustentation experiment, the field required to keep the particles attached to an electromagnet pole is linearly related with the total mass of the anionic counterion. In this way, we afford a method not only for the capture of anionic drugs but also for determining the amount of entrapped drug molecules in this class of innovative functional material, which makes it an inspirational example of the capabilities that supramolecularly assembled metal-organic materials can afford. Video S1 provides a fast insight into this novel magneto-sensing technique.

EXPERIMENTAL PROCEDURES

Resource availability

Lead contact

Further information and requests for resources and reagents should be directed to and will be fulfilled by the lead contact, Oscar Castillo (oscar.castillo@ehu.eus).

Materials availability

All of the unique reagents generated in this study are available from the lead contact with a completed materials transfer agreement.

Data and code availability

The accession number CCDC 2021699 for the supplementary crystallographic data of the compound reported in this article can be obtained free of charge via https://www.ccdc.cam.ac.uk/structures/search?, by e-mailing data_request@ccdc.cam.ac.uk or by contacting the Cambridge Crystallographic Data Centre (12 Union Road, Cambridge CB2 1EZ, UK; fax: +44-1223-336033). Otherwise, the published

article includes all of the important datasets generated or analyzed during this study. This study did not generate any code.

Synthesis of $[CrCu_6(\mu\text{-}H_2O)_6(\mu_3\text{-}OH)_6(\mu\text{-adeninato-}\kappa N3{:}\kappa N9)_6](SO_4)_{1.5}$

All of the chemicals were of reagent grade and were used as commercially obtained. Adenine (0.8 mmol, 0.108 g) was dissolved in a 20-mL water/methanol mixture (1:1 volume ratio), and was heated under continuous stirring for 20 min. Then, a 20-mL aqueous solution of Cu(II) sulfate pentahydrate (0.8 mmol, 0.200 g) and Cr(III) sulfate monohydrate (0.2 mmol, 0.078 g) was added. Immediately after, a green suspension was formed (pH 3.0). This suspension is dissolved through acidification with sulfuric acid until a light green solution was obtained at pH 1.5. Subsequently, the pH of the solution was shifted to 9.2 by adding triethylamine, and a green suspension was obtained, which was left in a crystallizer sealed with sealing film (Parafilm^M), slightly holed to allow the slow solvent evaporation. After 3 days, the suspension recrystallized as green needle-shaped crystals suitable for single-crystal X-ray diffraction analysis. Yield: 50%–60% (based on Cr). FTIR (KBr pellets, cm^{-1}): 3,388 vs, 3,200 sh, 1,642 vs, 1,603 vs, 1,548 s, 1,463 m, 1,402 m, 1,304 m, 1,277 m, 1,195 m, 1,152 m, 1,108 m, 1,033 w, and 935 w.

Single-crystal X-ray crystallography

The crystallographic data and details of the refinement parameters for compound $[CrCu_6(\mu\text{-}H_2O)_6(\mu_3\text{-}OH)_6(\mu\text{-adeninato-}\kappa N3{:}\kappa N9)_6](SO_4)_{1.5}$ are gathered in Table S2. All non-H atoms were refined anisotropically, except for those corresponding to disordered entities. The H atoms belonging to adeninato ligands have been geometrically fixed and refined according to a riding model with an isotropic thermal parameter linked to the atom to which they are attached (120%). The H atoms of the coordination water molecules and hydroxide groups have been located in the difference Fourier map or using the routine CALC-OH[32] implemented in the WinGX software suite.[33] The refinement of the latter H atoms has been performed with an isotropic thermal parameter of 150% with respect to their parent atom. Regarding the crystallization water molecules, not all of them could be placed in the Fourier map due to their high structural disorder; therefore, their contribution was removed using the SQUEEZE[34] procedure as implemented in PLATON[35] software. Accordingly, the H atoms of the located crystallization water molecules were not included due to this high disorder within the voids. During the structural resolution of the heptameric CrCu6 entity, the initial resolution showed anomalous elongated ellipsoids for a series of atoms attributed to the adeninato ligands. These large values of the thermal movements were related to a disorder implying 2 coplanar puric bases with inverted dispositions regarding the bridging mode (μ-$\kappa N3{:}\kappa N9$/μ-$\kappa N9{:}\kappa N3$). This disorder was modeled by refining the occupation of each part (A and B) and ensuring they add up to a total occupation factor of 1.

Crystal data: CCDC-2021699, $C_{30}H_{42}CrCu_6N_{30}O_{23}S_{1.5}$, M = 1,678.98, green needle, 0.11 × 0.05 × 0.03 mm, monoclinic, space group C2/c, a = 15.583(3) Å, b = 22.219(4) Å, c = 27.400(3) Å, β = 95.502(2)°, V = 9,300.0(3) $Å^3$, Z = 4, D_c = 1.199 g/cm^3, F000 = 3,365.4, μ = 3.295 mm^{-1}, T = 298(2) K, θ_{max} = 59.871°, 14,606 total reflections, 2,202 with I > 2σ(I), R_{int} = 0.0982, 6,738 data, 413 parameters, 40 restraints, GooF = 0.975, R = 0.1154 and wR = 0.3030 [I > 2σ (I)], R = 0.2132 and wR = 0.3765 (all reflections), −0.413 < Δρ < 0.661 e/$Å^3$.

Powder X-ray diffraction

The PXRD patterns were collected on a Phillips X'Pert Powder Diffractometer with copper Kα radiation. See more details on these measurements in Figure S14. Additional details can be found in the Supplemental experimental procedures.

Magnetic susceptibility and magnetization measurements

Magnetic measurements were performed on polycrystalline samples with a Quantum Design SQUID susceptometer covering the temperature range 5–300 K, at a magnetic field of 1,000 G. Magnetization as a function of the magnetic field (H) was measured using the same magnetometer in the $-50 \leq H/kOe \leq 50$ at 2 K after cooling the sample in zero field. See more details on these measurements in Figures S5 and S6.

Magnetic sustentation experiments

A Newport Pagnell England Electromagnet Type C sourced by a Hewlett Packard 6655A System DC Power Supply is used to provide a variable magnetic field under which the particles of the compound dispersed in methanol are attached to the lower end of the electromagnet pole until the magnetic field decreases enough for the gravitation to prevail and the particles to fall down. See more details on these measurements in Figures S8, S9, and S19 and Table S9.

Thermogravimetric characterization

Thermogravimetric measurements (TGA/differential thermal analysis [DTA]) were carried out in a METTLER TOLEDO TGA/SDTA851 thermal analyzer under a synthetic air atmosphere (79% N_2/21% O_2) with a flow rate of 50 cm^3/min, between 25°C and 800°C, with a heating rate of 5°C/min. See more details on these measurements in Figures S1, S11, and S17 and Tables S1, S5, and S8.

XPS

XPS measurements were performed on a SPECS system equipped with a Phoibos 150 1D-DLD analyzer and an Al Kα monochromatic radiation source. See more details on these measurements in Figure S18.

UV-visible (UV-vis) and FTIR spectroscopy

UV-vis spectra were recorded on a LAMBDA 850 spectrophotometer stabilized at 300 K. The absorbance was measured in Suprasil quartz cuvettes (10 mm, 3,500 mL). The IR spectra were recorded on a FTIR 8400S Shimadzu spectrometer in the 4,000–400 cm^{-1} spectral region. See more details on these measurements in Figures S13, S15, and S16 and Tables S5 and S6.

Elemental analyses

Elemental analyses (C, H, N) were performed on an Organic Elemental Thermo Scientific Modelo FLASH 2000 microanalyzer. The metal content was determined by inductively coupled plasma-atomic emission spectroscopy (ICP-AES) performed on a Horiba Yobin Yvon Activa spectrometer. See more details on these measurements in Table S7.

SUPPLEMENTAL INFORMATION

Supplemental information can be found online at https://doi.org/10.1016/j.xcrp.2021.100421.

ACKNOWLEDGMENTS

This work has been funded by the Universidad del País Vasco/Euskal Herriko Unibertsitatea (GIU17/50), the Gobierno Vas-co/Eusko Jaurlaritza (PIBA18/14; IT1291-19), the Ministerio de Economía y Competitividad (MAT2016-75883-C2-1-P), the Ministerio de Ciencia e Innovación (PID2019-108028GB-C21), and FEDER funds. Technical and human support provided by SGIker (UPV/EHU, MICINN, GV/EJ, and ESF) is also acknowledged.

AUTHOR CONTRIBUTIONS

R.P.A. performed the synthesis, chemical basic characterization, and drug capture experiments. B.A. performed the thermogravimetric characterization of the samples. G.B. and I.d.P. performed the electromagnet attraction experiments. O.C. and S.W. designed and supervised the research work. A.L. was in charge of the X-ray diffraction structural characterization, with support from S.P.-Y. S.P.-Y. wrote the original manuscript. All of the authors proofread, commented on, and approved the final manuscript for submission.

DECLARATION OF INTERESTS

The authors declare no competing interests.

Received: December 7, 2020
Revised: January 27, 2021
Accepted: April 6, 2021
Published: April 30, 2021

REFERENCES

1. Martinez, J.L. (2009). Environmental pollution by antibiotics and by antibiotic resistance determinants. Environ. Pollut. *157*, 2893–2902.

2. Geissen, V., Mol, H., Klumpp, E., Umlauf, G., Nadal, M., van der Ploeg, M., van de Zee, S.E.A.T.M., and Ritsema, C.J. (2015). Emerging pollutants in the environment: a challenge for water resource management. Int. Soil Water Conserv. Res. *3*, 57–65.

3. Gupta, V.K., Ali, I., Saleh, T.A., Nayak, A., and Agarwal, S. (2012). Chemical treatment technologies for waste-water recycling - an overview. RSC Advances *2*, 6380–6388.

4. Sophia A, C., and Lima, E.C. (2018). Removal of emerging contaminants from the environment by adsorption. Ecotoxicol. Environ. Saf. *150*, 1–17.

5. Dhaka, S., Kumar, R., Deep, A., Kurade, M.B., Ji, S.W., and Jeon, B.H. (2019). Metal–organic frameworks (MOFs) for the removal of emerging contaminants from aquatic environments. Coord. Chem. Rev. *380*, 330–352.

6. Jiao, L., Seow, J.Y.R., Skinner, W.S., Wang, Z.U., and Jiang, H.L. (2018). Metal–organic frameworks: Structures and functional applications. Mater. Today *27*, 43–68.

7. Eddaoudi, M., Kim, J., Rosi, N., Vodak, D., Wachter, J., O'Keeffe, M., and Yaghi, O.M. (2002). Systematic design of pore size and functionality in isoreticular MOFs and their application in methane storage. Science *295*, 469–472.

8. Lin, X., Jia, J., Hubberstey, P., Schroder, M., and Champness, N.R. (2007). Hydrogen storage in metal-organic frameworks. CrystEngComm *9*, 438–448.

9. Kalaj, M., and Cohen, S.M. (2020). Postsynthetic modification: an enabling technology for the advancement of metal–organic frameworks. ACS Cent. Sci. *6*, 1046–1057.

10. Ji, Z., Wang, H., Canossa, S., Wuttke, S., and Yaghi, O.M. (2020). Pore chemistry of metal-organic frameworks. Adv. Funct. Mater. *30*, 2000238.

11. Beobide, G., Castillo, O., Luque, A., and Pérez-Yáñez, S. (2015). Porous materials based on metal-nucleobase systems sustained by coordination bonds and base pairing interactions. CrystEngComm *17*, 3051–3059.

12. Loos, R., Tavazzi, S., Mariani, G., Suurkuusk, G., Paracchini, B., and Umlauf, G. (2017). Analysis of emerging organic contaminants in water, fish and suspended particulate matter (SPM) in the Joint Danube Survey using solid-phase extraction followed by UHPLC-MS-MS and GC-MS analysis. Sci. Total Environ. *607-608*, 1201–1212.

13. Chen, W.H., Lee, S.C., Sabu, S., Fang, H.C., Chung, S.C., Han, C.C., and Chang, H.C. (2006). Solid-phase extraction and elution on diamond (SPEED): a fast and general platform for proteome analysis with mass spectrometry. Anal. Chem. *78*, 4228–4234.

14. Bouri, M., Gurau, M., Salghi, R., Cretescu, I., Zougagh, M., and Rios, Á. (2012). Ionic liquids supported on magnetic nanoparticles as a sorbent preconcentration material for sulfonylurea herbicides prior to their determination by capillary liquid chromatography. Anal. Bioanal. Chem. *404*, 1529–1538.

15. Huang, D., Deng, C., and Zhang, X. (2014). Functionalized magnetic nanomaterials as solid-phase extraction adsorbents for organic pollutants in environmental analysis. Anal. Methods *6*, 7130–7141.

16. Naeimi, S., and Faghihian, H. (2017). Application of novel metal organic framework, MIL-53(Fe) and its magnetic hybrid: for removal of pharmaceutical pollutant, doxycycline from aqueous solutions. Environ. Toxicol. Pharmacol. *53*, 121–132.

17. Pérez-Aguirre, R., Beobide, G., Castillo, O., de Pedro, I., Luque, A., Pérez-Yáñez, S., Rodríguez Fernández, J., and Román, P. (2016). 3D Magnetically Ordered Open Supramolecular Architectures Based on Ferrimagnetic Cu/Adenine/Hydroxide Heptameric Wheels. Inorg. Chem. *55*, 7755–7763.

18. Pascual-Colino, J., Beobide, G., Castillo, O., da Silva, I., Luque, A., and Pérez-Yáñez, S. (2018). Porous supramolecular architectures based on π-stacking interactions between discrete metal-adenine entities and the non DNA theobromine/caffeine nucleobases. Cryst. Growth Des. *18*, 3465–3476.

19. Pascual-Colino, J., Beobide, G., Castillo, O., Lodewyckx, P., Luque, A., Pérez-Yáñez, S., Román, P., and Velasco, L.F. (2020). Adenine nucleobase directed supramolecular architectures based on ferrimagnetic heptanuclear copper(II) entities and benzenecarboxylate anions. J. Inorg. Biochem. *202*, 110865.

20. Li, J., Jiang, L., Chen, S., Kirchon, A., Li, B., Li, Y., and Zhou, H.C. (2019). Metal-Organic Framework Containing Planar Metal-Binding Sites: Efficiently and Cost-Effectively Enhancing the Kinetic Separation of C_2H_2/C_2H_4. J. Am. Chem. Soc. *141*, 3807–3811.

21. Blatov, V.A., Shevchenko, A.P., and Proserpio, D.M. (2014). Applied topological analysis of crystal structures with the program package topospro. Cryst. Growth Des. *14*, 3576–3586.

22. Pérez-Yáñez, S., Castillo, O., Cepeda, J., García-Terán, J.P., Luque, A., and Román, P. (2009). Analysis of the Interaction between Adenine Nucleobase and Metal-Malonato Complexes. Eur. J. Inorg. Chem. 3889–3899.

23. Leite Ferreira, B.J.M., Brandão, P., Dos Santos, A.M., Gai, Z., Cruz, C., Reis, M.S., Santos, T.M., and Félix, V. (2015). Heptacopper(II) and dicopper(II)-adenine complexes: synthesis, structural characterization, and magnetic properties. J. Coord. Chem. *68*, 2770–2787.

24. Liu, Z.-Y., Zhang, H.-Y., Yang, E.-C., Liu, Z.-Y., and Zhao, X.-J. (2015). A (3,6)-connected layer with an unprecedented adeninate nucleobase-derived heptanuclear disc. Dalton Trans. *44*, 5280–5283.

25. Zhong, Z.J., Matsumoto, N., Okawa, H., and Kida, S. (1991). Ferromagnetic dihydroxo-bridged Cr(III)-Cu(II) and Cr(III)-Cu(II)-Cr(III) complexes, [Cr(tet b)(OH) 2Cu(bpy)(CH3OH)](ClO4)3 and {Cu[Cr(tet b)(OH)2]2} (ClO4)4·H2O (tet b = racemic 5,7,7,12,14,14-hexamethyl-1,4,8,11-tetraazacyclotetradecane and bpy = 2,2′-bipyridine). Inorg. Chem. *30*, 436–439.

26. Azuah, R.T., Kneller, L.R., Qiu, Y., Tregenna-Piggott, P.L.W., Brown, C.M., Copley, J.R.D., and Dimeo, R.M. (2009). DAVE: a comprehensive software suite for the reduction, visualization, and analysis of low energy neutron spectroscopic data. J. Res. Natl. Inst. Stand. Technol. *114*, 341–358.

27. Kulkarni, S., Ramaswamy, B., Horton, E., Gangapuram, S., Nacev, A., Depireux, D., Shimoji, M., and Shapiro, B. (2015). Quantifying the motion of magnetic particles in excised tissue: effect of particle properties and applied magnetic field. J. Magn. Magn. Mater. *393*, 243–252.

28. Sun, W., Li, H., Li, H., Li, S., and Cao, X. (2019). Adsorption mechanisms of ibuprofen and naproxen to UiO-66 and UiO-66-NH2: Batch experiment and DFT calculation. Chem. Eng. J. *360*, 645–653.

29. Paunovic, O., Pap, S., Maletic, S., Taggart, M.A., Boskovic, N., and Turk Sekulic, M. (2019). Ionisable emerging pharmaceutical adsorption onto microwave functionalised biochar derived from novel lignocellulosic waste biomass. J. Colloid Interface Sci. *547*, 350–360.

30. Górny, D., Guzik, U., Hupert-Kocurek, K., and Wojcieszyńska, D. (2019). Naproxen ecotoxicity and biodegradation by Bacillus thuringiensis B1(2015b) strain. Ecotoxicol. Environ. Saf. *167*, 505–512.

31. Domínguez, J.R., González, T., Palo, P., and Cuerda-Correa, E.M. (2011). Removal of common pharmaceuticals present in surface waters by Amberlite XAD-7 acrylic-ester-resin: influence of pH and presence of other drugs. Desalination *269*, 231–238.

32. Nardelli, M. (1999). Modeling hydroxyl and water H atoms. J. Appl. Crystallogr. *32*, 563–571.

33. Farrugia, L.J. (2012). WinGX and ORTEP for Windows: an update. J. Appl. Crystallogr. *45*, 849–854.

34. Van der Sluis, P., and Spek, A.L. (1990). BYPASS: an effective method for the refinement of crystal structures containing disordered solvent regions. Acta Crystallogr. A *46*, 194–201.

35. Spek, A.L. (2009). Structure validation in chemical crystallography. Acta Crystallogr. D Biol. Crystallogr. *65*, 148–155.